metals

MDPI

Article

Microstructure and Tensile Properties of the Mg-6Zn-4Al-*x*Sn Die Cast Magnesium Alloy

Jin Zhou, Hamid Reza Jafari Nodooshan, Dejiang Li *, Xiaoqin Zeng * and Wenjiang Ding

National Engineering Research Center of Light Alloy Net Forming and Key State Laboratory of Metal Matrix Composite, Shanghai Jiao Tong University, Shanghai 200240, China; zhoujin1101@sjtu.edu.cn (J.Z.); hamidj_63@sjtu.edu.cn (H.R.J.N.); wjding@sjtu.edu.cn (W.D.)

* Correspondence: lidejiang@sjtu.edu.cn (D.L.); xqzeng@sjtu.edu.cn (X.Z.); Tel.: +86-21-54742301 (D.L. & X.Z.); Fax: +86-21-34203098 (D.L. & X.Z.)

Received: 9 January 2019; Accepted: 17 January 2019; Published: 23 January 2019

Abstract: The effect of various Sn contents (1–2 wt. %) on the microstructure, age hardening response, and tensile and casting properties of the high-pressure die cast Mg-6Zn-4Al alloy were studied. All as-cast alloys consisted of α-Mg and icosahedral quasi-crystalline phase; and the addition of 2% Sn caused the formation of Mg_2Sn phases. Dendrite structure and eutectic phases were observably refined by Sn addition. The hot tearing susceptibility of the die cast Mg-6Zn-4Al alloy prominently decreased with increasing Sn addition. During T6 heat treatment, Sn addition did not obviously affect the time to reach peak hardness, but significantly enhanced the age hardening response and improved the strength of alloys under peak-aged conditions. Compared to single aging, double aging resulted in the higher density of finer β_1' and β_2' precipitates. The double aged Mg-6Zn-4Al-1Sn alloy offered the optimum tensile properties among all conditions. The yield strength, ultimate tensile strength, and elongation were 209 MPa, 305 MPa, and 4.3%, respectively.

Keywords: Mg-Zn-Al-Sn; T6 treatment; microstructure; tensile properties; high pressure die casting

1. Introduction

In the past decades, magnesium alloys have been commonly used in automobile, aviation, and electronics industries owing to their excellent strength-to-weight ratios, good castability, and high specific stiffness [1,2]. Die casting is a very important fabrication way for Mg alloys, and has been extensively used to manufacture magnesium components due to its good size accuracy, high productivity, and significant economic benefit [3]. Unfortunately, widespread use of magnesium alloys in many areas is restricted by their moderate strength, low ductility, and expensive alloying elements [4–6]. As a result, for broader applications, it is necessary to research some low cost and high-strength die-castable Mg alloys.

The Mg-Zn-Al (ZA) series alloys are put forward as cost-effective and creep-resistant alloys to narrow the gap between AZ91D and some creep-resistant but expensive alloys [7]. However, the mechanical properties of the Mg-Zn-Al alloys still need to be enhanced. Alloying or micro alloying is an important method to improve mechanical properties of Mg alloys. It was reported that addition of rare earth (RE) to ZA alloys caused new RE-containing phases to form and microstructures were refined, which lead to the improvement of the mechanical properties of ZA alloys [8,9]. Adding small amount of Sr element also could refine the grain size and enhance the strength of ZA alloys [10]. Addition of Ca to ZA104 alloy could result in a harder and more stable intermetallic phase under high temperature, so that the creep resistance is improved substantially [11]. In recent years, Sn addition to ZA alloys get more concern, because it can achieve high strength at room and elevated temperature with low cost [12]. Yang et al. [13] illustrated that addition of Sn to gravity casting ZA84 magnesium alloy improves tensile,

creep properties, and casting fluidity. Chen et al. [14] have found that a slight addition of Sn (0.5 wt. %) lead to the improvement in the ambient and elevated temperature strength of ZA62 alloy.

In addition, many studies have been done to promote the effect of ageing strengthening for Mg-Zn-Al ternary alloys hardenable by precipitation [15–17]. The Mg-Zn-Al-Sn system is considered to be suitable for heat treatment to obtain high strength. Sasaki et al. [16] reported that peak hardness of Mg-2.2Sn-0.5Zn-1.0Al can be increased to 95 HV by double aging. It has been found that the Mg-6Zn-3Sn-2Al alloy after ageing has much greater strength than in the as-cast state [17].

However, some Mg-Zn-Al alloys are susceptible to hot tearing during solidification, which limited their applications in casting components [18]. Previous studies have revealed that Sn addition could improve castability of Mg alloys [13,19]. Turen found that, with addition of 0.5 wt. % Sn to AZ91 magnesium alloy, fluidity increased and hot tearing susceptibility (HTS) decreased [19].

The present study chooses Mg-6Zn-4Al as the base alloy owing to its moderate castability and outstanding age-hardening response. The HTS, microstructure, and tensile properties of Mg-6Zn-4Al-xSn (x = 0–2 wt. %) alloys were studied. The main aims of present work are to explore the effect of Sn addition and understanding the strengthening mechanism of T6-treated Mg-6Zn-4Al alloy containing Sn, so the results could be helpful for developing a new-style Mg-Zn-Al-Sn system alloy with excellent mechanical properties and better castability.

2. Experimental Procedures

High purity Mg (>99.9%), pure Zn (>99.95%), pure Al (>99.9%), and pure Sn (>99.9%) were used to fabricate alloys. A TOYO BD-350V5 (Toyo Machinery and Metal, Akashi, Japan) cold chamber high-pressure die casting machine was used to prepare a specific casting (as shown in Figure 1). All test samples were extracted from a plate-like bar (part E in Figure 1). The casting parameters adopted were as follows: 7.6 m/s injection speed, 680 °C melt temperature, and 200 °C mold temperature. In slow shot stage, injection speed was 0.25 m/s and 0.4 m/s. Speed was changed to 4 m/s in the fast shot stage. Casting pressure was 70 MPa.

The chemical compositions of investigated alloys were checked by an inductively-coupled plasma analyzer (ICP, Plasma 400, Perklin-Elmer, Waltham, MA, America) and listed in Table 1. The specimens were solution-treated for 40 h at 345 °C, and then quenched in the water. Single aging was performed at 175 °C in an oil bath. Double aging was held by pre-aging at 70 °C for 16 h, followed by aging at 175 °C. Vickers hardness (HV-30, Shanghai, China) measurement was made using 49 N load.

The hot tearing susceptibility was evaluated from the quantity of cracks in the different bars of the die castings. As shown in Figure 1, from bar A to bar E, the propensity of hot tearing was decreased. In order to increase hot tearing discrimination of different bars, a hot tearing factor of each bar was set (A:2, B = 4, C:8, D:16, E:32). The values of HTS were calculated by $\sum(Q_{tear} \times F_{bar})$, where Q_{tear} is the quantity of cracks on each bar and F_{bar} is the hot tearing factor of each bar. In order to ensure the credibility of the statistical results, ten die casting specimens were counted for each alloy and the average value reported.

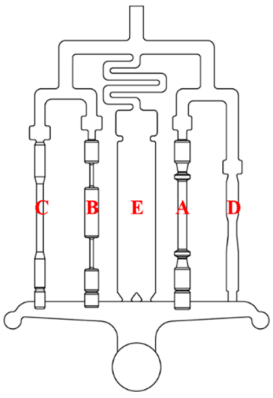

Figure 1. Schematic of die casting specimens.

For microstructure observation, as-cast samples were etched with 4% nitric acid plus alcohol solution and heat-treated samples were etched with solution picric acid (4.2 g picric acid + 10 mL water + 10 mL acetic acid + 70 mL ethanol). The microstructure observation was performed using a ZEISS optical microscope (OM, Zeiss Axio Observer A1, ZEISS, Jena, Germany), transmission electron microstructure (TEM, JEM-2100F, JEOL, Tokyo, Japan), and scanning electron microscopy (SEM, NOVA Nano 230, FEI, Hillsboro, OR, America). The dendrite sizes of the as-cast samples were evaluated on the OM images using Image-Pro Plus software by the linear intercept method. The TEM foils were made by combination of twin-jet electro-polishing and ion thinning. The composition of the phases was characterized with an energy dispersive spectrometer (EDS) installed in SEM. The phases of as-cast samples were identified by X-ray diffraction (XRD, D/max 2550VL/PC, Rigaku, Japan) operated at 5 °/min. Tensile tests (Z100, Zwick, Worms, Germany) were performed at a speed of 1 mm/min at room temperature (RT).

Table 1. Chemical compositions of the experimental alloys in weight percentage.

Alloy	Nominal Composition	Actual Composition (wt. %)			
		Zn	Al	Sn	Mg
ZA64	Mg-6Zn-4Al-0Sn	6.164	3.970	-	Bal
ZAT641	Mg-6Zn-4Al-1Sn	6.666	4.153	1.036	Bal
ZAT642	Mg-6Zn-4Al-2Sn	6.526	4.105	2.097	Bal

3. Results and Discussion

3.1. Hot Tearing

A previous study has pointed out that ZA64 alloys are prone to hot tearing during die casting [20]. For further application of ZA series alloys, the hot tearing susceptibility of the alloys needs to be improved. Figure 2 shows the hot tearing susceptibility of the investigated die cast alloys by addition of Sn content. It is obvious that, with increasing Sn addition to ZA64 alloy, HTS decreases. The typical images of die casting ZA64 and ZAT642 alloys are shown in Figure 3. The cracks in the ZA64 alloy are shown by head arrow in Figure 3a. It can be seen from Figure 3b that there was no obvious crack in the die casting specimen of ZAT642 alloy. It is interesting that Sn addition could significantly improve the hot tearing susceptibility of die casting the ZA64 alloy, which reveals that Mg-6Zn-4Al-*x*Sn alloys are promising for die casting, but the mechanism for the effect of Sn on HTS of the ZA64 alloy will be further studied in another work.

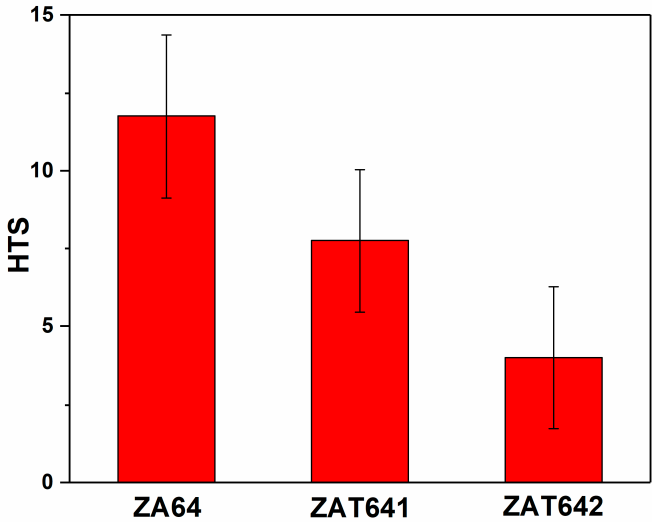

Figure 2. Hot tearing susceptibility (HTS) of die casting Mg-6Zn-4Al-*x*Sn alloys.

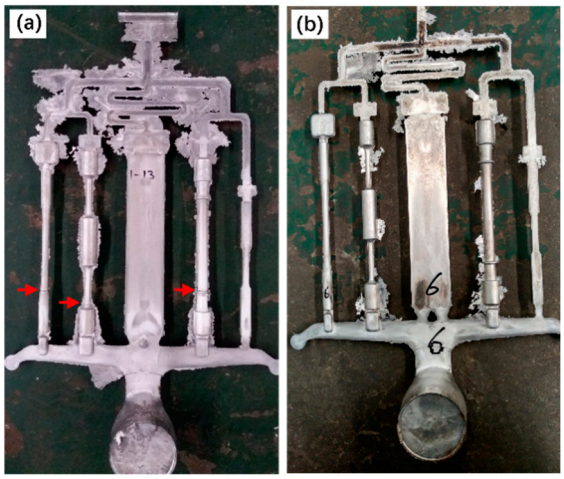

Figure 3. Appearance of the specimens of die-cast (**a**) ZA64 and (**b**) ZAT642 alloys.

3.2. As-Cast Microstructure

The optical microstructures of the as-cast Mg-6Zn-4Al-*x*Sn alloys are shown in Figure 4. The microstructure displayed a dendritic solidification structure composed of α-Mg and a lot of second phases at the dendritic boundaries and in inter-dendritic spacings. With Sn addition, the dendrite size decreased considerably and the dendrite structure tended to become equiaxed morphology. The average dendrite sizes of ZA64, ZAT641, and ZAT642 were 15.79 ± 2.5 μm, 12.61 ± 1.6 μm, and 10.37 ± 1.2 μm, respectively, which implies that Sn addition refines the dendrite structure of the as-cast ZA64 alloy. On the basis of solidification theory, solute segregation is a key factor on the dendrite refinement [21,22]. During solidification process, Sn atoms enrich at the solid–liquid interface and accelerates the solute enrichment of Al and Zn [23], which causes a composition undercooling in front of the solidification interface resulting in the dendritic refinement.

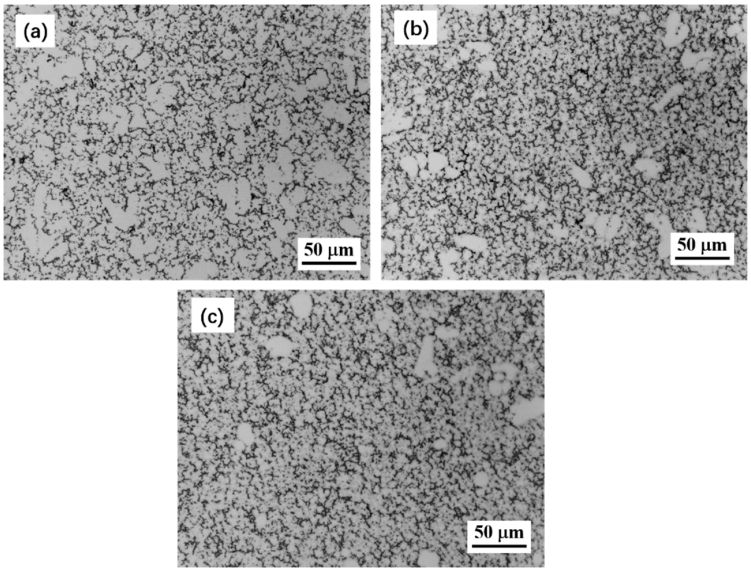

Figure 4. Optical micrographs of the as-cast Mg-6Zn-4Al-*x*Sn alloys: (**a**) ZA64, (**b**) ZAT641, and (**c**) ZAT642.

The XRD patterns of the all as-cast alloys are presented in Figure 5. Constituent phases in alloys are mainly α-Mg phases and quasicrystal phases (I-phase). With 2% Sn addition, diffraction peak of Mg_2Sn phases could be detected. Generally, when the difference of the electronegativity between different elements is higher, the formation of intermetallic compounds is easier. According to this theory, Mg_2Sn phases were easily formed in the Mg-Zn-Al-Sn system referring to the electronegative

values of Mg, Al, Zn, and Sn (1.31, 1.61, 1.65, and 1.96, respectively) [14]. However, diffraction peaks of Mg_2Sn in ZAT641 alloy cannot be observed, because Sn atoms mostly dissolve into the matrix. Referring to existing literature [24], Mg_2Sn phases can easily be detected when the addition of Sn is above 2% in as-cast Mg-Zn-Al alloys, which is consistent with the present work.

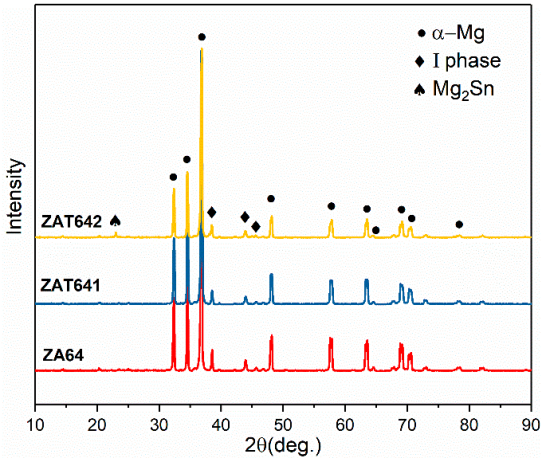

Figure 5. X-ray diffraction (XRD) results of the as-cast Mg-6Zn-4Al-*x*Sn alloys.

To further verify the presence of I-phase, the ZA64 alloy was examined by using TEM analysis. Figure 6 illustrates TEM morphology of the second phases and corresponding selected-area electron diffraction (SAED) patterns. As shown in SAED patterns, intermetallic phases displayed a five-fold symmetry, which could be identified as the icosahedral quasi-crystalline structure. I-phase had the approximate chemical composition of $Mg_{47}Zn_{29}Al_{24}$ and $Mg_{47}Zn_{32}Al_{21}$ in the ZA64 alloy, which were similar to the result reported by Bourgeois [25]. Zhang et al. [26] found that low Zn-Al ratio and high Al contents are easier to lead to the appearance of I-phase in casting ZA alloys, which supports the existence of I-phases in this study. It is widely accepted that I-phase has excellent properties, for instance high strength, high thermal conductivity, and low friction coefficient [27–29]; moreover, I-phase–matrix interface has a good bonding and could contribute to transfer stress between two phases [30]. However, formation mechanism of I-phase in ZA system alloys still need to be further studied.

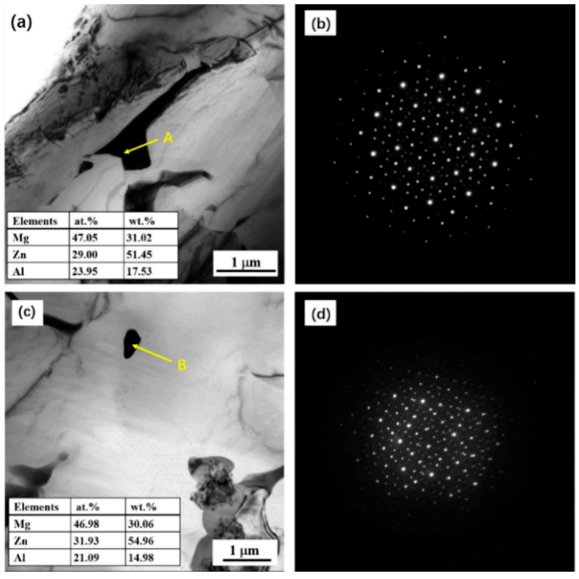

Figure 6. Bright-field transmission electron microscopy (TEM) images of I-phases (**a**) and (**c**) in the Mg-6Zn-4Al alloy; (**b**) and (**d**) are the corresponding selected area diffraction (SAED) patterns. The insets are the corresponding energy-dispersive X-ray spectroscopy (EDS) results.

Figure 7 shows the typical SEM microstructures of all of the as-cast studied alloys. Most of the continuous and/or quasi-continuous network I-phases were distributed along the grain boundaries. It was obvious that eutectic phases were refined by Sn addition; however, compared with the ZAT641 alloy, intermetallics tended to become coarse and were distributed continuously again with 2% Sn addition. Previous studies reported that the size of eutectics is closely related to the morphology of primary dendrite [31]. As shown above, addition of 1% Sn decreases the size of α-Mg dendrite and second dendrite arm spacing, which will provide limited regions for the growth of eutectics, leading to the refinement of the eutectics. With 2% Sn addition, more solutes concentrate at the solid–liquid interface, promoting the growth of eutectics, which causes eutectics to grow with continuous and coarse morphology.

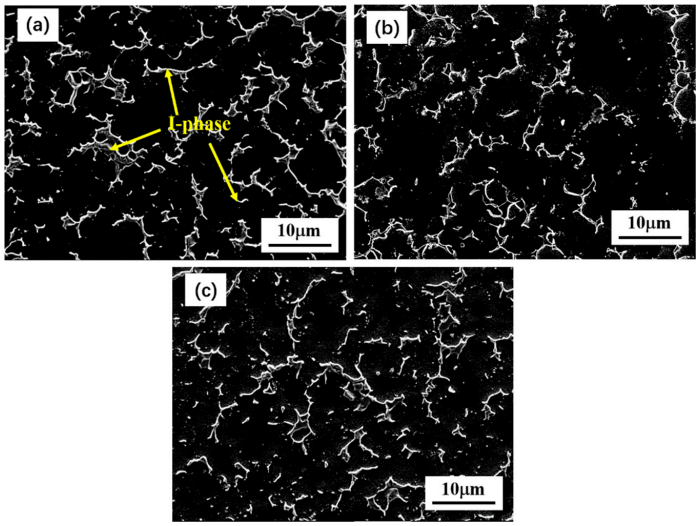

Figure 7. Scanning electron microscopy (SEM) micrographs in the as-cast Mg-Zn-4Al-*x*Sn alloys: (**a**) ZA64, (**b**) ZAT641, and (**c**) ZAT642.

According to EDS mapping results, as shown in Figure 8, the Sn element was mainly distributed in Mg_2Sn, and Mg_2Sn phases mainly coexisted with the continuous phase. However, Zn and Al elements were mainly enhanced in the I-phase.

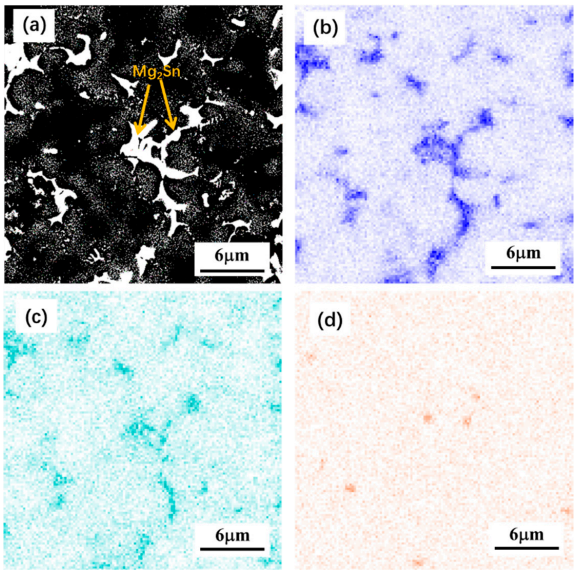

Figure 8. Back-scattered electronic image (**a**) and EDS element distribution of: (**b**) Zn, (**c**) Al, and (**d**) Sn in the as-cast ZAT642 alloy.

3.3. Aging Response Behavior and Peak-Aged Microstructure

Figure 9 shows the age hardening response of all of the studied alloys subjected to single aging and double aging. The hardness values increased with aging time in the early stage and then decreased due to over-aging. Various Sn addition had no significant influence on the time to reach peak hardness. Obviously, Sn addition substantially enhanced the age hardening response. As the Sn content increased from 0% to 2%, peak hardness increased from 80 to 89 Hv after single aging, and increased from 90 to 98 Hv after double aging. Compared to single aging, the double aging treatment resulted in a significant increase in the hardness and accelerated the age-hardening process.

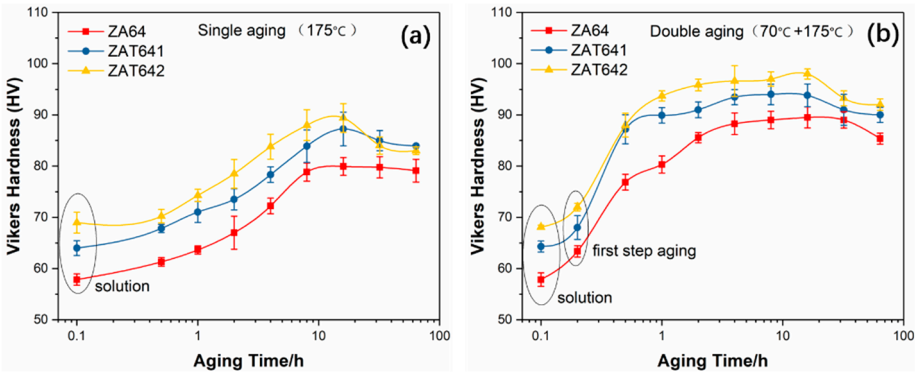

Figure 9. Aging-hardening curves of the Mg-6Zn-4Al-*x*Sn alloys: (**a**) single aging, and (**b**) double aging.

Figure 10 shows the optical micrographs of all double-peak aged alloys. There were still a small number of undissolved intermetallics distributed along grain boundaries and within grains. There was no significant difference in grain size among all double-peak aged alloys.

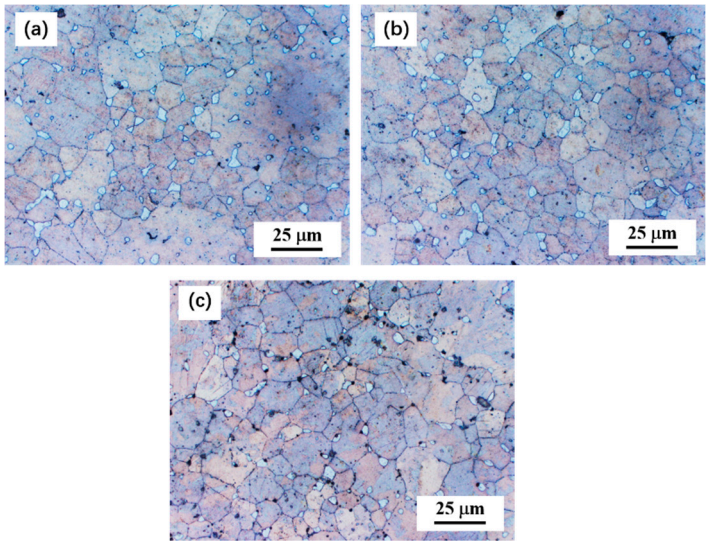

Figure 10. Optical images of the double-peak aged alloys: (**a**) ZA64, (**b**) ZAT641, and (**c**) ZAT642.

From Figure 11a, the SEM image of the double-peak aged ZAT642 alloy shows that some spherical (marked A) and irregularly shaped (marked B) phases were distributed on the grain boundaries and within grains. According to EDS analysis, as shown in Figure 11b,c, spherical and irregularly shaped phases belonged to Mg_2Sn and undissolved I-phases, respectively.

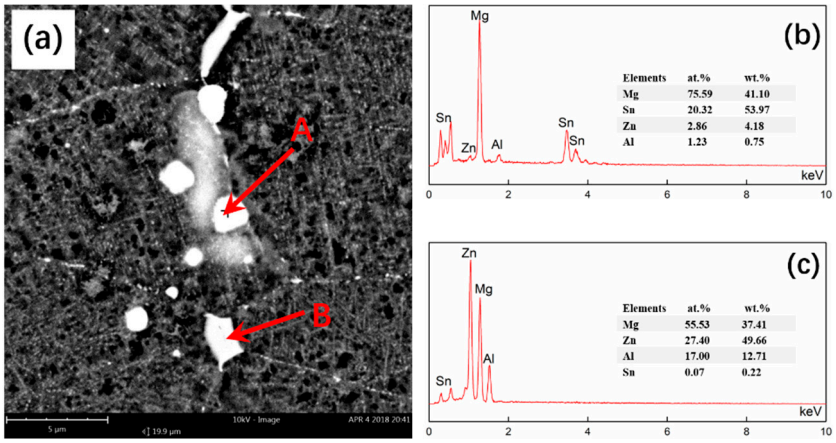

Figure 11. SEM image and EDS results of the aged ZAT642 alloy. (**a**) SEM microstructure, and (**b**,**c**) EDS spectrums detected from the points A and B in (**a**).

Figure 12 shows the TEM images of all double-peak aged alloys obtained from $[10\bar{1}0]$ zone axis. Densely distributed precipitates presented two different morphologies. One was rod precipitates, aligned with the $[0001]_{Mg}$ direction, and the other was coarse plate precipitates, lying on the (0001) basal plane. Rod-like precipitates was identified as β_1' phase, and plate-like precipitates was β_2' phase, which are typical precipitates in the Mg-Zn system. It is commonly known that β_1' has an orientation relationship of $\{2\bar{1}\bar{1}0\}_{\beta'_1}//(0001)_{Mg}$ and $[0001]_{\beta'_1}//[0001]_{\beta'_1}$ with the matrix, and β_2' phase has a $\{2\bar{1}\bar{1}0\}_{\beta'_2}//\{10\bar{1}0\}_{Mg}$ and $[0001]_{\beta'_2}//[0001]_{Mg}$ orientation relationship [32–34]. In the double-peak aged ZA64 alloy, precipitates were coarse and distributed randomly. Adding Sn to the ZA64 alloy resulted in the prominent refinement and homogenous distribution of β_1' and β_2' precipitates, especially with 1% Sn addition. The precipitates in the ZAT641 alloy were much denser and finer than those in ZA64 alloys. The size of the rod-like precipitates was ~60.4 nm and ~6.8 nm in length and diameter, and the diameter and width of the blocky precipitate was ~24.6 nm and ~17.1 nm, respectively, in the double-peak aged ZAT641 alloy.

The results obviously show that Sn addition can enhance the age-hardening response. Previous investigation concluded that adding Sn to Mg-Zn alloys leads to co-segregation of Zn and Sn atoms in precipitates after double aging. The atomic radius of Zn was similar to that of Sn. The interfacial misfit energy between the precipitate and the matrix by the size effect was reduced due to combination of Sn and Zn elements in the precipitates, which was beneficial for the age hardening response [35]. Therefore, precipitates were noticeably denser and finer in as-aged Sn-containing alloys compared to the ZA64 alloy. For the ZAT642 alloy, most of the Sn atoms participate in the formation of Mg_2Sn phases, distributing along the grain boundaries rather than existing in the precipitates. Thus, the precipitates in the ZAT642 alloys were not as dense and fine as those in the ZAT641 alloy.

The TEM bright-field images of single-peak aged and double-peak aged ZAT641 alloys taken from the $[11\bar{2}0]$ zone axis are shown in Figure 13. It was apparent that the double aging treatment brought about finer, more uniform, and higher-density precipitates compared to the single aged alloy. This is ascribed to the emergence of Guinier Preston (G.P) zones during pre-aging. It was reported that G.P zones form under low-temperature aging conditions in Mg-Zn-Al systems [36]. G.P. zones could act as heterogeneous nucleation points for the transition phases during the next stage of high temperature aging, thus leading to homogeneous distribution of finer precipitates and enhancing the age-hardening response [37].

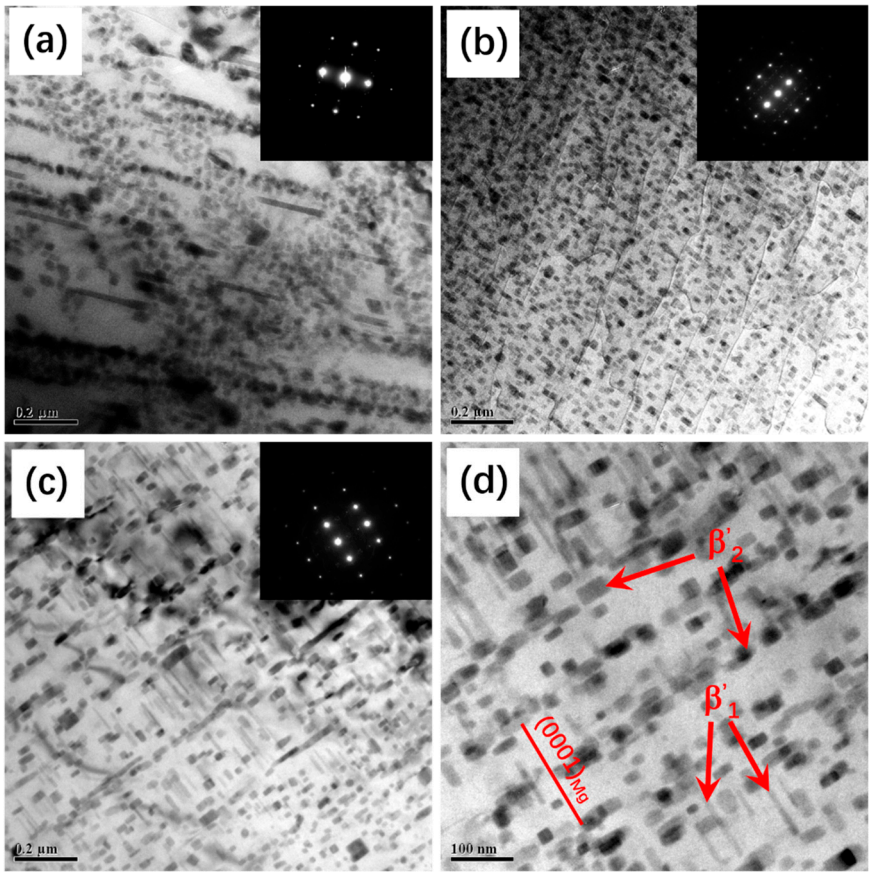

Figure 12. Bright-field TEM images of double-peak aged alloys taken from $[10\bar{1}0]$ zone axis: (**a**) ZA64, (**b**) ZAT641, (**c**) low, and (**d**) high magnification of ZAT642.

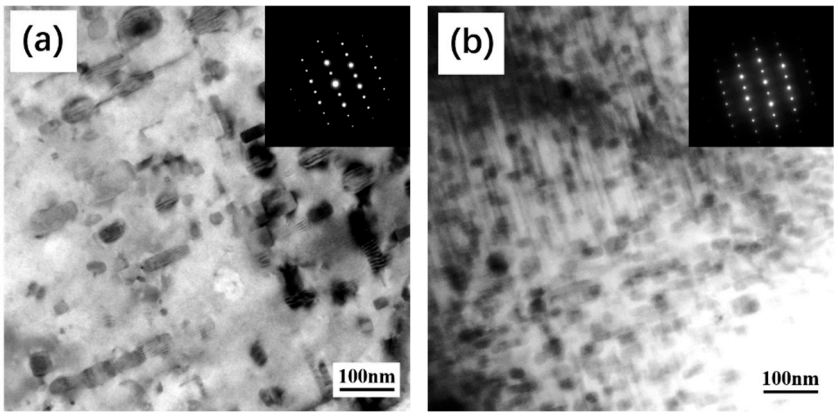

Figure 13. Bright-field TEM images of peak-aged ZAT641 taken from the $[11\bar{2}0]$ zone axix: (**a**) single ageing, and (**b**) double aging.

The bright TEM image of coarse particle A, at the grain boundary, in the double-aged ZAT642 alloy is shown in Figure 14. According to the EDS result inserted in Figure 14, particle A can be identified as the cubic Mg_2Sn phase. The size of the Mg_2Sn phase was about 500 nm, much larger than precipitates. These Mg_2Sn phases did not dissolve into the matrix due to their high temperature stability, and they could contribute to the increase of base hardness of the ZAT642 alloy, as shown in Figure 9.

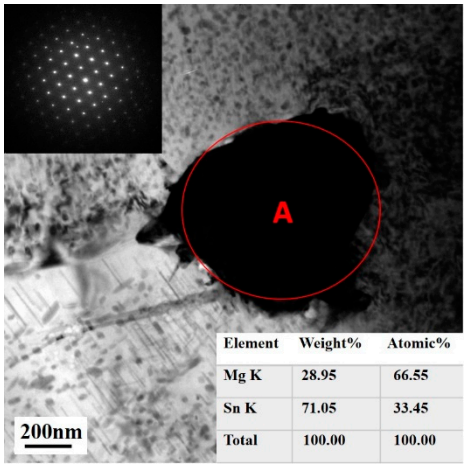

Figure 14. Bright-field TEM image of a representative inter-dendritic Mg_2Sn particle. Inset image is the corresponding selected area diffraction pattern recorded along $[110]_{Mg2Sn}$. Inset table is the corresponding EDS result.

3.4. Tensile Properties

Figure 15 shows the tensile test results of all alloys in as-cast and peak-aged states. For the as-cast alloys, Sn addition improved the yield strength (YS) and ultimate tensile strength (UTS) of the ZA64 alloy. The YS of the as-cast alloys increased moderately with increasing Sn content, which should be ascribed to the following aspects. Sn addition refines dendrite and eutectic phases. As we know, fine and uniform phases along the grain boundaries are more likely to be an effective barrier to suppress dislocation movement so as to improve the YS [38]. Additionally, Sn atoms have high solubility in the Mg matrix, resulting in solute strengthening, and Mg_2Sn phases in the ZAT642 alloy could contribute to the improvement of YS. However, the ZAT641 alloy offered the highest UTS and elongation, which was 228 MPa and 4.1%, respectively. When Sn addition was up to 2%, eutectic phases and Mg_2Sn phases tend to coexist with I-phases, becoming coarse and continuous or quasi-continuous in morphology, which caused a slight loss of the UTS and ductility.

Compared to the as-cast alloys, T6 treatments remarkably enhanced the YS and UTS of all the studied alloys, especially after the double aging treatment. Moreover, as-aged Sn-containing alloys showed more obvious age-strengthening effect than the ZA64 alloy. Among all of the as-aged alloys, the ZAT641 alloy offered the optimal aging response. The YS and UTS of the double-peak aged ZAT641 samples were 209 MPa and 305 MPa, respectively, which were almost 24 MPa and 18 MPa higher than that of the double-peak aged ZA64 alloy. Meanwhile, compared with the single aged ZAT641 alloy, the YS got improvement of 36MPa after the double ageing treatment.

As we can see from Figure 10, after the ageing treatment, the grain size was not decreased obviously by various Sn addition. Accordingly, precipitation strengthening was most possibly considered as the main reason for the strengthening of as-aged alloys. During the heat treatment process, most of the compounds dissolved into the matrix, through solution treatment, and subsequent aging brought about abundant β_1' and β_2' precipitates within the Mg matrix, effectively suppressing the dislocation movements and consequently strengthening the as-cast alloys. As is well known, the distribution and volume fraction of precipitates has a great effect on the strength of age-treated Mg alloys [39]. The increment in critical resolved shear stress (CRSS) caused by dislocations bowing around particles in a slip plane is inversely proportional to λ, and in turn λ is proportional to $R/\sqrt{fv}$ (λ is the effective average particle spacing, R is the mean planar particles size, and fv is the volume fractions of the particles) [40]. Double aged ZAT641 samples had denser, finer, and more uniformly distributed precipitates; therefore, they exhibited higher strength than other alloys.

It must also be mentioned that the UTS and elongation of the alloy containing 2% Sn were deteriorated. As it can be seen from Figures 11 and 14, there were coarse Mg_2Sn phases and undissolved

second phases in the peak-aged ZAT642 alloy, which possibly caused stress concentration and acted as crack initiation sites, causing an adverse effect on the UTS and elongation of the ZAT642 alloy.

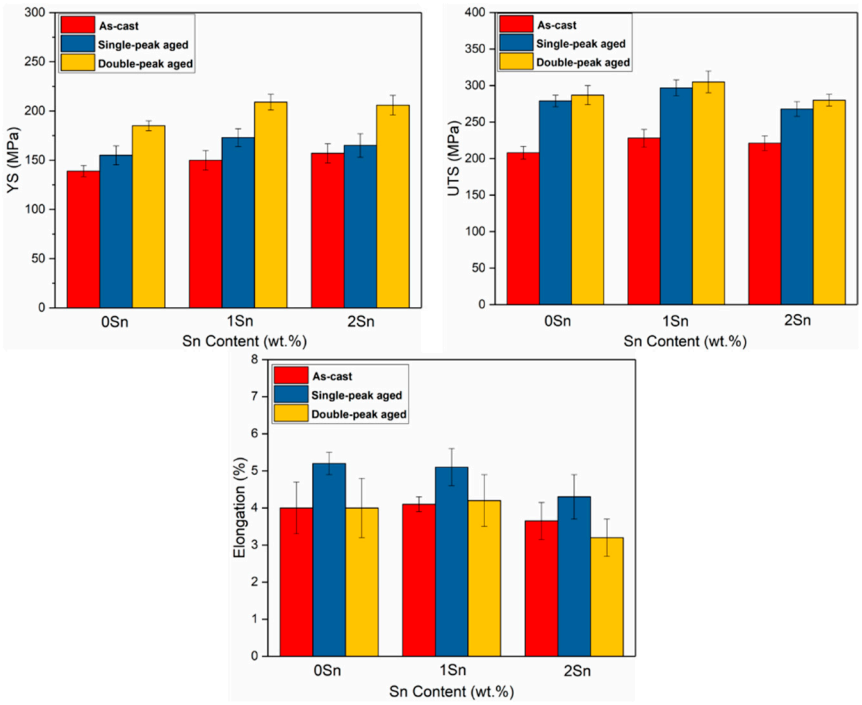

Figure 15. Mechanical properties of as-cast, single-peak aged and double-peak aged Mg-6Zn-4Al-*x*Sn alloys. (**a**) Yield strength, (**b**) ultimate tensile strength, and (**c**) elongation.

Fracture surface characteristics were performed on SEM to investigate the fracture mode of as-aged alloys. SEM fractographs of all double-peak aged alloys are shown in Figure 16. Generally speaking, most magnesium alloys possess hexagonal crystal structure and fewer slip systems, two or more slip systems barely activated simultaneously. Fracture modes of magnesium alloys are usually cleavage fractures, quasi-cleavage fractures, and inter-granular fractures [41]. From Figure 16, cleavage facets and steps, river patterns, and fine dimples can be clearly observed, which demonstrates that fracture surfaces had a mix of the fracture modes mentioned above. With various Sn addition, the fracture mode was not altered remarkably. However, the cleavage planes were large and the river patterns were obvious in the ZA64 alloy, as shown in Figure 16a. By comparison, the ZAT641 alloy had less cleavage planes and obvious fine dimples (Figure 16b), indicating that the ductility of ZAT641 was relatively high, which was in line with the elongation results. As seen from Figure 16c, there were visible microcracks in the ZAT642 alloys, which was presumably related to the existence of the undissolved Mg_2Sn and irregular residual phases distributing along grain boundaries. Generally, cracks easily originate and extend along the interfaces between the α-Mg matrix and coarse phases due to stress concentration, and coarse Mg_2Sn phases and undissolved eutectics provide effective crack initiation sites. Besides, the fractured surface of ZAT642 also displayed the evident micro-void, which are created by the process of void coalescence at the initial stage of fracture coalescence in the areas showing higher density particles. Therefore, the ductility and UTS of the as-aged ZA642 alloy were relatively poor.

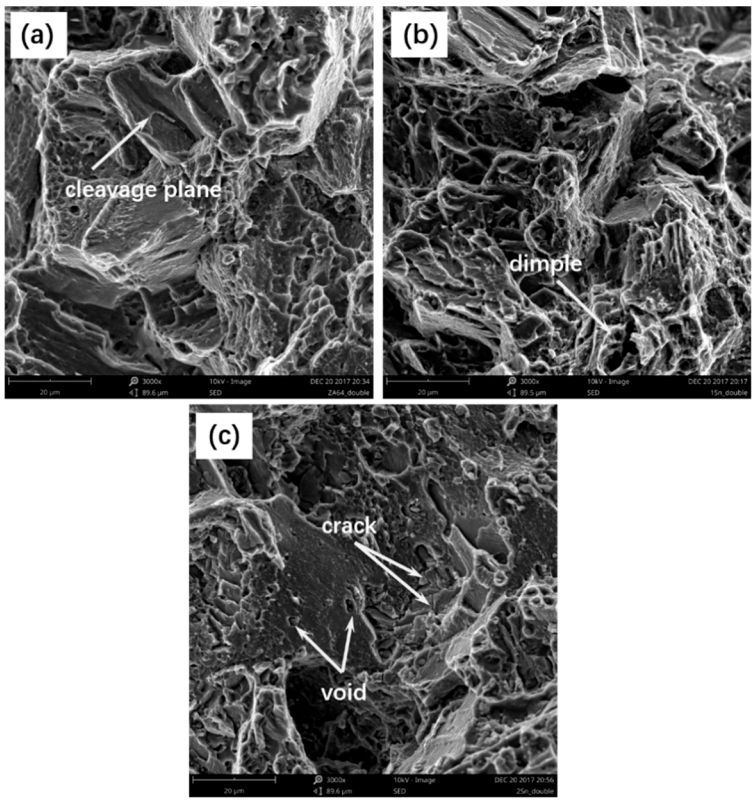

Figure 16. The SEM images of the tensile fracture surface of the double-peak aged alloys: (**a**) ZA64, (**b**) ZAT641, and (**c**) ZAT642.

4. Conclusions

The microstructure and mechanical properties of as-cast and as-aged Mg-6Zn-4Al-*x*Sn (*x* = 0–2 wt. %) alloys, as well as castability, were studied. The following results were drawn:

(1) As-cast ZA64 alloys are composed of α-Mg and icosahedral quasi-crystal phase. Sn addition substantially refine eutectic phases. Mg_2Sn phases can be detected when the content of Sn is 2%.

(2) Sn addition obviously decreases the hot tearing susceptibility of the die cast ZA64 alloy. The hot tearing susceptibility of the 2% Sn-containing alloy is much lower than the ZA64 die casting alloy.

(3) Sn addition improves the strength and ductility of the as-cast ZA64 alloy, due to eutectics refinement and solute strengthening. The ZAT641 alloy offers optimal tensile properties in the as-cast condition.

(4) T6 treatment significantly improves the strength of studied alloys, especially double aging, which is mainly attributed to precipitate strengthening and homogeneous distribution of denser and finer precipitates in double aged samples.

(5) Sn addition results in more β_1' and β_2' phase precipitates, and refinement of precipitates during aging, so as to enhance the strength of as-aged alloys. The double-aged ZAT641 alloy exhibits the best comprehensive mechanical properties with a YS of 209 MPa, UTS of 305 MPa, and elongation of 4.3%, whereas the addition of 2% Sn deteriorates the ultimate tensile strength and elongation of as-aged alloys because of the coarse Mg_2Sn phases along the grain boundary.

Author Contributions: Supervision, H.R.J.N, D.L. and X.Z.; writing—original draft preparation, J.Z.; investigation, J.Z. and H.R.J.N.; conceptualization, H.R.J.N. and J.Z.; writing—review and editing, D.L., X.Z., and H.R.J.N.; project administration, W.D.

Acknowledgments: The National Key R&D Program (No.2016YFB0301002) supported by the Ministry of Science and Technology of China and the Major Science and Technology projects in Qinghai province (2018-GX-A1) is acknowledged. This work was co-funded by the National Natural Science Foundation of China (numbers

51301107 and 51601111). D. Li acknowledges the financial support received from Shanghai Jiao Tong University through the SMC-Young scholar program.

Conflicts of Interest: The authors declare no conflicts of interest.

References

1. Mordike, B.L.; Ebert, T. Magnesium: Properties-applications-potential. *Mater. Sci. Eng. A* **2001**, *302*, 37–45. [CrossRef]
2. Furuya, H.; Kogiso, N.; Matunaga, S.; Senda, K. Applications of magnesium alloys for aerospace structure systems. *Mater. Sci. Forum* **2000**, *350*, 341–348. [CrossRef]
3. Otarawanna, S.; Laukli, H.I.; Gourlay, C.M.; Dahle, A.K. Feeding mechanisms in high-pressure die castings. *Metall. Mater. Trans. A* **2010**, *41*, 1836–1846. [CrossRef]
4. Ye, H.Z.; Liu, X.Y. Review of recent studies in magnesium matrix composites. *J. Mater. Sci.* **2004**, *39*, 6153–6171. [CrossRef]
5. Zhang, D.F.; Hu, H.J.; Pan, F.S.; Yang, M.B.; Zhang, J.P. Numerical and physical simulation of new SPD method combining extrusion and equal channel angular pressing for AZ31 magnesium alloy. *Trans. Nonfer. Met. Soc. China* **2010**, *20*, 478–483. [CrossRef]
6. Qi, F.; Zhang, D.; Zhang, X.; Xu, X. Effect of Sn addition on the microstructure and mechanical properties of Mg–6Zn–1Mn (wt.%) alloy. *J. Alloys Compd.* **2014**, *585*, 656–666. [CrossRef]
7. Liu, Y.; Qian, M.; Fan, Z. Microstructure and mechanical properties of a rheo-diecast Mg-10Zn-4.5 Al alloy. *Mater. Trans.* **2005**, *46*, 2221–2228. [CrossRef]
8. Wang, Y.X.; Guan, S.K.; Zeng, X.Q.; Ding, W.J. Effects of RE on the microstructure and mechanical properties of Mg–8Zn–4Al magnesium alloy. *Mater. Sci. Eng. A* **2006**, *416*, 109–118. [CrossRef]
9. Xiao, W.L.; Jia, S.S.; Wang, L.D.; Wu, Y.M.; Wang, L.M. The microstructures and mechanical properties of cast Mg–Zn–Al–RE alloys. *J. Alloys Compd.* **2009**, *480*, L33–L36. [CrossRef]
10. Luo, X.H.; Xu, C.X. Effects of Sr on the microstructure and mechanical properties of Mg-10Zn-4Al-0.3 Mn alloy. *Foundry* **2015**, *4*, 013.
11. Zhang, Z.; Tremblay, R.; Dube, D. Microstructure and mechanical properties of ZA104 (0.3–0.6 Ca) die-casting magnesium alloys. *Mater. Sci. Eng. A* **2004**, *385*, 286–291. [CrossRef]
12. Wang, B.; Pan, F.S.; Chen, X.H.; Guo, W.; Mao, J.J. Microstructure and mechanical properties of as-extruded and as-aged Mg–Zn–Al–Sn alloys. *Mater. Sci. Eng. A* **2016**, *656*, 165–173. [CrossRef]
13. Yang, M.B.; Pan, F.S. Effects of Sn addition on as-cast microstructure, mechanical properties and casting fluidity of ZA84 magnesium alloy. *Mater. Des.* **2010**, *31*, 68–75. [CrossRef]
14. Chen, J.H.; Chen, Z.H.; Yan, H.G.; Zhang, F.Q.; Liao, K. Effects of Sn addition on microstructure and mechanical properties of Mg–Zn–Al alloys. *J. Alloys Compd.* **2008**, *461*, 209–215. [CrossRef]
15. Pan, H.C.; Ren, Y.P.; Fu, H.; Zhao, H.; Wang, L.Q.; Meng, X.Y.; Qin, G.W. Recent developments in rare-earth free wrought magnesium alloys having high strength: A review. *J. Alloy. Compd.* **2016**, *663*, 321–331. [CrossRef]
16. Sasaki, T.T.; Oh-Ishi, K.; Ohkubo, T.; Hono, K. Effect of double aging and microalloying on the age hardening behavior of a Mg-Sn-Zn alloy. *Mater. Sci. Eng. A* **2011**, *530*, 1–8. [CrossRef]
17. Chen, J.H.; Chen, Z.H.; Yang, H.G.; Zhang, F.Q. Microstructural characterization and mechanical properties of a Mg–6Zn–3Sn–2Al alloy. *J. Alloys Compd.* **2009**, *467*, L1–L7. [CrossRef]
18. Easton, M.A.; Abbott, T.B.; Nie, J.F.; Savage, G. An assessment of high pressure die cast Mg-Zn-Al alloys. In *Magnesium Technology 2008: Proceedings of Symposium, New Orleans, Louisiana, USA, 9–13 March 2008*; Minerals, Metals & Materials Society (TMS): Warrendale, PA, USA, 2008.
19. Turen, Y. Effect of Sn addition on microstructure, mechanical and casting properties of AZ91 alloy. *Mater. Des.* **2013**, *49*, 1009–1015. [CrossRef]
20. Xiao, W.L.; Easton, M.A.; Zhu, S.M.; Dargusch, M.S.; Gibson, M.A.; Jia, S.S.; Nie, J.F. Casting defects and mechanical properties of high pressure die cast Mg-Zn-Al-RE *Alloys Adv. Eng. Mater.* **2012**, *14*, 68–76.
21. Kim, Y.M.; Wang, L.; You, B.S. Grain refinement of Mg-Al cast alloy by the addition of manganese carbonate. *J. Alloys Compd.* **2010**, *490*, 695–699. [CrossRef]
22. Lee, Y.C.; Dahle, A.K.; StJohn, D.H. The role of solute in grain refinement of magnesium. *Metall. Mater. Trans. A* **2000**, *31*, 2895–2906. [CrossRef]

23. Dong, X.G.; Fu, J.W.; Wang, J.; Yang, Y.Y. Microstructure and tensile properties of as-cast and as-aged Mg-6Al-4Zn alloys with Sn addition. *Mater. Des.* **2013**, *51*, 567–574. [CrossRef]
24. Wang, B.; Chen, X.H.; Pan, F.S.; Mao, J.J. Effects of Sn addition on microstructure and mechanical properties of Mg-Zn-Al alloys. *Prog. Nat. Sci. Mater. Int.* **2017**, *27*, 695–702. [CrossRef]
25. Bourgeois, L.; Mendis, C.L.; Muddle, B.C.; Nie, J.F. Characterization of quasicrystalline primary intermetallic particles in Mg-8wt% Zn-4wt% Al casting alloy. *Philos. Mag. Lett.* **2001**, *81*, 709–718. [CrossRef]
26. Zhang, J.; Guo, Z.X.; Pan, F.S.; Li, Z.S.; Luo, X.D. Effect of composition on the microstructure and mechanical properties of Mg–Zn–Al alloys. *Mater. Sci. Eng. A* **2007**, *456*, 43–51. [CrossRef]
27. Wollgarten, M.; Beyss, M.; Urban, K.; Liebertz, H.; Köster, U. Direct evidence for plastic deformation of quasicrystals by means of a dislocation mechanism. *Phys. Rev. Lett.* **1993**, *71*, 549–552. [CrossRef]
28. Dubois, J.M.; Kang, S.S.; Stebut, J.V. Quasicrystalline low-friction coatings. *J. Mater. Sci. Lett.* **1991**, *10*, 537–541. [CrossRef]
29. Yoshida, T.; Itoh, K.; Tamura, R.; Takeuchi, S. Plastic deformation and hardness in Mg–Zn–(Y, Ho) icosahedral quasicrystals. *Mater. Sci. Eng. A* **2000**, *294*, 786–789. [CrossRef]
30. Yuan, G.Y.; Amiya, K.; Kato, H.; Inoue, A. Structure and mechanical properties of cast quasicrystal-reinforced Mg–Zn–Al–Y base alloys. *J. Mater. Res.* **2004**, *19*, 1531–1538. [CrossRef]
31. Nave, M.D.; Dahle, A.K.; StJohn, D.H. Eutectic growth morphologies in magnesium–aluminum alloys. In *Magnesium Technology 2000: Proceedings of the Symposium, Nashville, TN, USA, 12–16 March 2000*; Minerals, Metals & Materials Society (TMS): Warrendale, PA, USA, 2000.
32. Oh-Ishi, K.; Hono, K.; Shin, K.S. Effect of pre-aging and Al addition on age-hardening and microstructure in Mg-6 wt% Zn alloys. *Mater. Sci. Eng. A* **2008**, *496*, 425–433. [CrossRef]
33. Mendis, C.L.; Oh-ishi, K.; Hono, K. Effect of Al additions on the age hardening response of the Mg–2.4Zn–0.1Ag–0.1Ca (at.%) alloy-TEM and 3DAP study. *Mater. Sci. Eng. A* **2010**, *527*, 973–980. [CrossRef]
34. Hall, E.O. The age-hardening characteristics of two magnesium-zinc alloys. *J. Inst. Metals* **1968**, *96*, 21–27.
35. Wei, S.H.; Zhu, T.P.; Hou, H.B.; Kim, J.H.; Kobayashi, E.; Sato, T.; Hodgson, M.; Gao, W. Effects of Pb/Sn additions on the age-hardening behaviour of Mg–4Zn alloys. *Mater. Sci. Eng. A* **2014**, *597*, 52–61. [CrossRef]
36. Takahashi, T.; Kojima, Y.; Takanishi, K. Study of precipitates in an aged Mg-3.6 wt% Zn alloy by an X-ray method. *J. Jpn. Inst. Light Met.* **1973**, *23*, 376–382. [CrossRef]
37. Wang, J.; Liu, R.D.; Luo, T.J.; Yang, Y.S. A high strength and ductility Mg-Zn-Al-Cu-Mn magnesium alloy. *Mater. Des.* **2013**, *47*, 746–749. [CrossRef]
38. Balasubramani, N.; Pillai, U.T.S.; Pai, B.C. Optimization of heat treatment parameters in ZA84 magnesium alloy. *J Alloys Compd.* **2008**, *457*, 118–123. [CrossRef]
39. Friedrich, H.E.; Mordike, B.L. *Magnesium Technology: Metallurgy, Design Data, Applications*; Springer: Berlin, Germany, 2006; pp. 77–79.
40. Mendis, C.L.; Bettles, C.J.; Gibson, M.A.; Gorsse, S.; Hutchinson, C.R. Refinement of precipitate distributions in an age-hardenable Mg-Sn alloy through microalloying. *Philos. Mag. Lett.* **2006**, *86*, 443–456. [CrossRef]
41. Wei, S.H.; Zhu, T.P.; Michael, H.; Gao, W. Effects of Sn addition on the microstructure and mechanical properties of as-cast, rolled and annealed Mg-4Zn alloys. *Mater. Sci. Eng. A* **2013**, *585*, 139–148. [CrossRef]